Inhibition of Asphaltene Aggregation using Deep Eutectic Solvents: COSMO-RS Calculations and Experimental Validation

Nikhil Kumar[1,♣] , Mood Mohan[2,3,♣], Jeremy C. Smith[2,4], Blake A. Simmons[3,5], Seema Singh[3], Tamal Banerjee[1,*]

[1] Department of Chemical Engineering, Indian Institute of Technology Guwahati, Guwahati, Assam, 781039, India

[2] Biosciences Division and Center for Molecular Biophysics, Oak Ridge National Laboratory, Oak Ridge, Tennessee 37831, United States

[3] Deconstruction Division, Joint Bioenergy Institute, 5885 Hollis Street, Emeryville, California 94608, United States

[4] Department of Biochemistry and Cellular and Molecular Biology, University of Tennessee, Knoxville, Tennessee 37996, United States

[5] Biological Systems and Engineering Division, Lawrence Berkeley National Laboratory, 1 Cyclotron Road, Berkeley, California 94720, United States

♣ N.K. and M. M. contributed equally to this work.

[*]Corresponding Author(s):

E-mail: tamalb@iitg.ac.in;
Tel: +91-361-2582266,
Fax: +91-361-2690762

Abstract

Asphaltene precipitation/deposition adversely affects various oil and gas processes, such as oil recovery, transportation, and petroleum processing. The resulting increase in viscosity of crude oil decreases distillate yields creating unstable phase separation. Deep Eutectic Solvents (DESs) have recently gained interest as inhibitors of asphaltene aggregation. The goal of the present study is to derive the mechanism of inhibition of petroleum asphaltene aggregation by a novel screening of DESs. An Archipelago based chemical structure of asphaltene was adopted for performing quantum chemical calculations. The structure was used in the COSMO-RS (Conductor-like Screening Model for Real Solvents) model to screen potential DESs for asphaltene precipitation. It was found that DESs containing thymol were the most promising of the 153 DES combinations screened. The COSMO-RS predictions were validated experimentally using solubility data of asphaltene in DESs. Among the studied DESs, thymol-diphenyl ether provided the highest solubility for asphaltene, which was further validated using the experimental and the COSMO-RS predicted data. In addition, to characterize the structural interactions between asphaltene and DESs, Fourier Transform Infrared (FTIR) spectroscopy and Nuclear Magnetic Resonance (NMR) measurements were performed. It was found that strong interaction between asphaltene and the DESs is responsible for the higher asphaltene dispersion. The present approach opens pathways to rationally design and understand the impact of structural variation of DESs based on their interactions with asphaltene.

Keywords: Asphaltene, Deep Eutectic Solvents, COSMO-RS, Solubility, FTIR, NMR.

1. Introduction

Crude oil is composed of variety of hydrocarbons, of which the main constituents comprise saturates, asphaltene, resins, and aromatics (SARA components). Among the SARA components, the heaviest, asphaltene is problematic in terms of processing and transportation in the energy sector [1]. Asphaltene tends to precipitate during transportation, plugging the downstream pressure vessels and blocking reservoir porosity. Although variable in chemical structure, asphaltenes share common structural attributes, *i.e.*, strong aromaticity, high polarity, a low H/C ratio, and the inclusion of heteroatoms (*e.g.*, S, N, and O) and porphyrin (a complex ring system). Asphaltene also contains a high number of alkyl chains attached to their aromatic rings and possesses strong intramolecular van der Waals interactions, hydrogen bonds [2] π–π stacking [3, 4], electrostatic interactions, and repulsive steric interactions [5-8]. These strong intramolecular interactions between the asphaltenes molecules itself are also responsible for aggregation and are perhaps the least understood aspect of asphaltene structure. The polycyclic aromatics, heteroatoms, and polar functional groups in asphaltene also have a role in bulk flow characteristics. Aggregation starts during crude oil recovery and transportation when pressure, temperature, and chemical variations alter the crude oil thermodynamic stability [9, 10].

The transportation and refinement of asphaltene crude oil as a feedstock is a critical challenge in the global oil and gas sector. In an attempt to avoid the aggregation that occurs in crude oil production, research has been undertaken to investigate the chemical nature of asphaltene. Mutelet *et al.* [11] reported that petroleum asphaltene could act as a strong hydrogen-bond acceptor but a weak hydrogen bond donor. Furthermore, Wu *et al.*[12] studied the interaction between asphaltene, resin and crude oil by considering resins and asphaltene as solutes dispersed in crude oil with the effect of varying temperature and pressure.

The high mass resolving power and mass accuracy of (Fourier Transform Ion Cyclotron Resonance Mass Spectrometry) FT-ICR MS allow for the resolution and elemental composition assignment of thousands of species in petroleum-derived materials [13]. FT-ICR MS was used recently for the application in various studies focusing on heavy crude oils, associated production deposits, and isolated asphaltenes to reflect recent advances in the characterization of complex mixtures, as well as low-resolution mass spectrometry experiments aimed at verifying suspected multimer formation.

Stability and aggregation inhibition of asphaltene in crude oil can be achieved by using a variety of organic solvents such as toluene and xylene [13, 14]. However, these aromatic

solvents are volatile and harmful to the environment. Trials of alternative solvents such as amines and alkyl benzene sulfonic acid significantly enhanced asphaltene precipitation inhibition *via* acid-base interactions. However, the asphaltene-amphiphilic interactions involved are electrophilic addition reactions, leading to irreversible bond formation between acid-bases and precipitates in the non-polar medium. Recently, ionic liquids (ILs) have been proven to be potential solvents for asphaltene inhibition aggregation; however, the cost of ILs is high and multiple steps are involved in the complex IL synthesis process. Alternatively, resinous organic polymers can prevent asphaltene aggregation by adsorbing onto the surface of asphaltene molecules and creating steric hindrance[14]. They are oil-soluble, but their efficacy and usefulness have been questioned. Altogether, there is no economical technique to prevent asphaltene aggregation in different crude oil operations.

In 2003, Abbott *et al.* [15] first developed DESs, which are formed through two or more compounds capable of forming a strong hydrogen bond network between hydrogen bond acceptor (HBA) and hydrogen bond donor (HBD) molecules, resulting in a considerable negative deviation of the melting temperature of the mixture from the individual component melting points[16]. In recent years, DESs have emerged as promising replacements for ILs in a wide variety of research areas and industries[17], including CO_2 capture, biomass processing, nanotechnology, extraction processes[18-21], electrochemistry, catalysis, and other applications[22-24]. DESs are generally referred to as analogues of ionic liquids (ILs). They have a wide range of structural diversity and desirable features, including high thermal and chemical stability, low volatility, non-flammability, and non-toxicity. Several DES combinations form a clear transparent liquid in ambient conditions and can be employed as solvents in various applications.

The economic and environmental aspects of the process regarding the amount of solvent utilized increased the importance of solvent recyclability[25]. For example, regenerating the DES reduces costs and prevents the use of substantial amounts of DESs in every purifying startup[26]. The regeneration experiment comprises three major steps: (1) conducting the single-stage extraction, (2) washing or back-extraction where the regeneration solvents are used to capture the impurities within the DES, and (3) the evaporation of impurities from the DES-rich phase to recover the pure DES.

Minimizing the makeup of solvents used is critical in the implementation of any separation process for an economic and long-term sustainable approach. The potential three different

schemes for the reuse and recycling of the DESs can be implemented in the future study. Therefore, DES recycling has gained importance from different aspects, and many publications have discussed the most effective recyclability methods, and the problems arises due to stability of ionic liquids and deep eutectic solvents[27, 28].

For asphaltene precipitation inhibition Kashefi *et al.* [29] prepared the choline chloride ([Ch]Cl) and phenylacetic acid DES at a 1:1 molar ratio. They concluded that on the basis of both microscopic and particle size measurements, the best asphaltene inhibitor was octyl phenol with 500 mg/L optimum concentration. Further, Jahangiri *et al.* [30] also studied the inhibition of asphaltene precipitation using the [Ch]Cl and monoethylene glycol (1:1) DESs. They observed that DES as an inhibitor able to increase the resistance of asphaltene against precipitation caused by the addition of an aliphatic solvent. Rashid *et al.* [31] conducted COSMO-RS (Conductor-like Screening Model for Real Solvents) calculations to screen some of ionic liquids for asphaltene solubility. For these calculations, a model structure of asphaltene was considered consisting of a polycyclic aromatic moiety with a highly polar functional groups (=O, CHOO, –N<, etc.). This was attached to combined seven aromatic rings representing island model of asphaltene to mimic the polar asphaltene structure as available in crude oil. Recently, Sanati *et al.*[32] studied the comparison of ionic liquids and hydrophobic DES for the inhibition of asphaltene precipitation and reported that hydrophobic DESs are effective solvents for asphaltene precipitation inhibition.

A systematic screening of DESs for asphaltene solubility has not been performed, but is necessary, as experimental screening is time-consuming, expensive, and impractical. An associated challenge is that the precise and accurate chemical structure of the complex asphaltene remains unresolved. The present study focuses on screening deep eutectic solvents for asphaltene precipitation inhibition using the COSMO-RS model. In addition, the study also aims to derive an accurate molecular model structure for computational calculations. The derived chemical structure of asphaltene was confirmed by performing Fourier transform infrared (FTIR) spectroscopy and quantum chemical calculations. Several combinations of HBAs and HBDs of DESs were screened using the COSMO-RS quantum chemical model by calculating thermodynamic properties and ranking the solvents based on their interaction capability. Thereafter, experimental solubility measurements were performed to test the COSMO-RS results, and the recovered asphaltene was further characterized using FTIR and

nuclear magnetic resonance (NMR) techniques, providing an understanding of molecular interactions and the solubility mechanism of asphaltene in DES.

2. Computational Details

2.1 Quantum Chemical and COSMO-RS Calculations

The initial chemical structures of asphaltene, HBA, and HBDs of DES were drawn using Gauss view 5.0 [33]. The geometries of all molecules were optimised at B3LYP (Becke 3-parameter hybrid DFT functional combined with the Lee-Yang–Parr correlation) theory with functional incorporating the dispersion correction 3-D basis set, namely 6-311+G (d, p), using the *Gaussian*09 package [34]. Frequency calculations were also carried out to ensure that the optimized structures were at energy minima. After successful molecular optimization, the BVP86/TZVP/DGA1 level of theory and basis set was used to generate the COSMO file (Figure S1). Here, the COSMO-RS calculations were carried out to screen the 153 combinations of HBAs and HBDs of DESs for asphaltene solubility i.e., inhibition of precipitation. The HBAs and HBDs of DESs are selected based on the different chemical functionalities, hydrophilicity, and hydrophobicity. For example, thymol, menthol, decanoic acid based DESs are hydrophobic. After screening, experimental solubility measurements were performed to test the COSMO-RS results. The generated COSMO files were further used as input to the BIOVIA COSMOTherm (version 21.0, Dassault Systems) package with BP_TZVP_21 parametrization [35]. Using the COSMO-RS model, the logarithmic activity coefficient (ln (γ)) and excess enthalpy (H^E) of binary mixtures, i.e., asphaltene and DESs were calculated, and the mole fraction of asphaltene and DESs are set to 0.2 and 0.8, respectively.

The logarithmic activity coefficient (ln(γ)) of component *i* is related to the chemical potential μ_i is given as the following equation [36, 37].

$$\ln(\gamma_i) = \left(\frac{\mu_i - \mu_i^0}{RT} \right) \tag{1}$$

where μ_i^0 is the chemical potential of the pure component *i*, *R* and *T* are the ideal gas constant and absolute temperature. The excess enthalpy (H^E) of a binary mixture was calculated using equation (2) [36, 38].

$$H_M^E = \sum x_i H_i^E = \sum x_i \left[H_{(i,mixture)} - H_{(i,pure)} \right] \tag{2}$$

where H_m^E is the excess enthalpy of the mixture, defined as the enthalpy difference between component *i* in the mixture and in the pure state, and the total excess enthalpy of a mixture is the algebraic sum of electrostatic (misfit), hydrogen bonding, and van der Waals interactions.

3. Experimental Solubility Measurements for Asphaltene

3.1 Materials

In the present study, asphaltene was extracted from crude oil acquired from local Oil Industry at Guwahati, India. The other chemicals used for the present study are given in Table S1 and were used as received from the supplier without further purification.

3.2 Preparation of DESs

The DESs were prepared by mixing the hydrogen bond acceptor (HBA: thymol) and hydrogen bond donors (HBDs: diphenyl ether, biphenyl, and camphor) at specific molar ratios from 1:1 to 7:3 (Figure S2). The HBA and HBD mixture were placed in the flat bottom flask and heated in an oil bath at 333.15 ± 0.01 K with a constant stirring speed of 350 rpm until a transparent liquid was formed [39]. The detailed procedure to prepare the DESs is given elsewhere [19]. The obtained DESs were vacuum dried at 0.51 bar and 335.15 K overnight to remove any moisture content. The viscosities of the four solvents are given in Figure S3.

3.3 Extraction of Asphaltene from Crude Oil

Asphaltene was extracted by adding heptane to crude oil in a 40:1 v/v volumetric ratio under ambient conditions by following the ASTM recommended procedure for separating asphaltene from crude oil (ASTM D2007-80) [40]. The mixture was then filtered under vacuum using 0.2 μm pore size Whatman filter paper. Further, the filter cake was repeatedly washed with *n*-heptane to remove any resins until the effluent from the filter became colourless. Finally, the asphaltene sample was kept overnight at room temperature, then converted to powder form, and vacuum oven-dried at 0.51 bar (333.15 K, 24 hr) to remove any remaining impurities and water content. The resulting asphaltene sample was then placed in an airtight vial and stored in a dry place at ambient conditions for further experimental use.

3.4 Asphaltene Solubility Assays

Solubility was measured by adding an excess amount of asphaltene to 1 ml of DESs at 298.15 K and atmospheric pressure. The vials were sealed and placed in an aluminum block holder. This was transferred to a heating plate temperature control (PT100) with a magnetic stirrer (series H03D from LBX Instruments). The mixtures were magnetically stirred at a constant

450 rpm for at least 12 hrs. After reaching saturation solubility, which means dispersion stops after a certain amount and precipitation starts at the bottom of the vial, the stirring was stopped, and the excess solid was allowed to settle down for 5-6 hrs. After saturation, the asphaltene and DES mixture were filtered using polytetrafluoroethylene filters (0.2 μm pore size) to remove the undissolved fraction of asphaltene. All solubility tests were performed in duplicate to confirm the accuracy.

The asphaltene solubility was calculated using equation 3, where m_{ASP} and m_{DES} represent the weight of asphaltene dispersed in DES and pure DESs, respectively.

$$Asp\ wt. = \frac{m_{Asp}}{m_{DES+Asp}} \times 100 \quad (3)$$

3.5 Characterization of Recovered Asphaltene

3.5.1 Nuclear Magnetic Resonance (NMR)

NMR analysis (Bruker Advance-600 MHz instrument, Germany) was performed to measure the purity of the prepared DESs and the interaction between asphaltene and DESs after dissolution. 10-20 μL of the sample was dissolved in 0.6 mL of DMSO-d_6 or $CdCl_3$, placed in the NMR tubes, and properly sealed with a cap and paraffin. The NMR spectrometer of 11.74 T (600 MHz response of ^{1}H and 2D NMR) was used to record the NMR spectral analysis. Further, the ^{1}H NMR of neat DESs and DESs + asphaltene mixture are given in supplementary information (Figure S4-S7). The chemical shifts for the deuterated solvents DMSO-d_6 and $CdCl_3$ were obtained at 2.5 ppm and 7.27 ppm and used as the references in the spectrum.

3.5.2 Fourier Transform Infrared (FTIR) Spectroscopy

The Fourier transform infrared (FTIR) spectroscopy was performed to understand structural changes in the asphaltene before and after the addition of DESs using the Perkin Elmer Spectrum 6700 with a horizontal Golden Gate attenuated total reflection (ATR) with diamond crystals installed. The samples were analysed using FTIR spectroscopy with a resolution of 4 cm^{-1} and 32 scans per sample over the wave number range of 4000–400 cm^{-1}.

4. Results and Discussions

4.1 Structure of Asphaltene

Density-functional theory (DFT) is a powerful tool in computational quantum chemistry modeling that is used to investigate the electronic structure of many-body systems, in particular

atoms, molecules, and condensed phases. Over the past few years, significant progress has been achieved in developing novel DFT techniques that can be used in existing quantum-chemical computing systems. In addition, IR spectroscopic DFT calculations aid in deriving accurate molecular structure by characterizing the vibrational frequencies of the different functional groups that are present in experimentally obtained FTIR spectra.

Chemical structures of asphaltene used are shown in Figure 1. These structures were calculated using the archipelago model of Mullins [41]. According to this archipelago model, as shown in Figure 1b and 1c, asphaltene molecules consist of a collection of smaller, polyaromatic compounds linked together in a non-linear, branched structure containing polar heteroatoms. The choice of chemical models is critical when performing the COSMO-RS calculations, especially applying it to screen DESs for asphaltene. We performed quantum chemical calculations to calculate the IR spectra of different asphaltene model structures and compared it with the experimental FTIR spectra. Based on the IR spectra and elemental compositions, the model structure (2 and 3 in Figure 1) of asphaltene was selected for further COSMO-RS screening. Quantum chemical (QC) calculations were then performed on the archipelago-based structure for the screening of DESs with COSMO-RS. The complete details of the IR spectra calculations using DFT are discussed elsewhere [42, 43].

Figure 2 shows the experimental recorded FTIR spectrum and the theoretically calculated IR spectrum of asphaltene obtained with the B3LYP/6-311+G (d, p) level of theory and basis set. For QC-based IR calculations, three different model structures of asphaltene were considered, as shown in Figure 1. Model 1 was taken from Rashid *et al.* (2019)[25], and model 2 and 3 asphaltene structures were taken from Badu *et al.*[44]. All the significant experimentally recorded IR spectra vibrations are correctly described in the QC calculated IR spectrum for the model 2 and model 3 asphaltene structures; however, model 1 shows more significant deviation from the experimentally measured vibrations. The absorption peak at 1750-1780 cm^{-1} corresponds to the stretching C=O, and the peak at 1890-1900 cm^{-1} corresponds to the stretching of carboxylate groups >COOH, which is absent in experimental, model 2, and model 3 IR spectrums. The stretching vibrations for the various groups, *i.e.*, O─H, C─H, N=H, C=O, C─C, C─H_3, and C─H_2, can be observed in Figure 2. The O─H and N─H group vibrations have a characteristic range of 3000–3600 cm^{-1} and appear as a characteristic peak for DES and asphaltene respectively. These are mainly responsible for the strong hydrogen bonding interaction between DESs and asphaltene [45]. The O─H or N─H stretching vibrations were found to be in a specific range of 3200-3600 cm^{-1} for the model structure of

asphaltene. Excellent agreement was obtained between the theoretically predicted frequencies for the O─H/N─H vibration and experimentally obtained FTIR spectra[46, 47]. The C=O bond interaction of the asphaltene molecule was found to be in the range of 1600-1800 cm^{-1}.

Moreover, the elemental analysis of asphaltene was reported in Table 1. The H/C atomic ratio of computational model 2 and model 3 structures of asphaltene is close to the experimental elemental analysis compositions calculated using the ^{1}H NMR. Model 1, in contrast, has a lower H/C molar ratio and higher oxygen and nitrogen contents, which leads to a less compatible model structure for molecular simulations. COSMO-RS is a powerful computational approach to calculating thermodynamic properties and screening solvents for solute dissolution. To predict the solubility and thermodynamic properties, the COSMO-RS model requires structural information on the solvent and solute. COSMO-RS predicted thermodynamics properties such as $ln(\gamma)$ (related to the solubility) and H^E (related to the interaction energies) are important parameters determining the capability of a solvent to dissolve a solute. According to solid-liquid equilibria assumptions **[48, 49],** the reciprocal of the activity coefficient (γ) and H^E characterizes solute solubility in the respective solvent. Thus, solutes with lower $ln(\gamma)$ and H^E (*i.e.*, more negative) in the solvents indicate that the solvent has a greater tendency to interact and solubilize the solute. In our earlier works, we showed the applicability of COSMO-RS for calculating activity coefficients (γ) and predicting biopolymer/plastics solubility in ionic liquids and validated the approach against a set of experimentally studied systems [50-53].

As a benchmark study using the three model asphaltene structures, COSMO-RS calculations were performed to investigate the solubility of asphaltene in ionic liquids and organic solvents. Figure 3 shows the COSMO-RS predicted $ln(\gamma)$ plotted against known experimental asphaltene solubilities. From Figure 3, it is observed that the model 2 and model 3 structures show an excellent correlation between the COSMO-RS calculated $ln(\gamma)$ and the experimental solubility, but model 1 shows a contrary behavior. Therefore, from this benchmarking study, models 2 and 3 structures of asphaltene again represent more accurate and reasonable chemical structures for asphaltene and were thus adopted for DESs screening calculations.

4.2 Screening of Deep Eutectic Solvents for Asphaltene

From the above discussions, it is clear that models 2 and 3 are reliable model structures for asphaltene and thus these were used in COSMO-RS calculations to screen DESs. For these calculations, 153 DESs were screened at room temperature (298.15 K) and atmospheric

pressure. The results of DES screening for asphaltene are provided in Table S2. In Figure 4, DESs are sorted according to their dissolving capacity and arranged in such a way that DESs with high dissolving power (i.e., more negative values of $ln(\gamma)$ and $H^E << 0$) of asphaltene are situated in the left side of Figure 4, and the weaker ones (*i.e.*, less negative or positive values of $ln(\gamma)$ and H^E) are situated on the right side.

From the COSMO-RS screening data, we established a rule of thumb for high asphaltene solubility as H^E value ≤ 0.26 and $ln(\gamma) \leq -0.51$. These cut-off values were selected by benchmarking the H^E and $ln(\gamma)$ values for the asphaltene model structures with conventional solvents such as toluene and xylene, chosen for the benchmarking because they are industrially used to dissolve the heavy fraction of crude oil. From the screening results, hydrophobic DESs such as thymol:diphenyl ether (1:1), thymol:biphenyl (1.6:1), biphenyl:cadaverine (1:5.66), 2-methylquinoline:cadaverine (1:3.34), thymol:decanoic acid (3:2 and 1:1), and thymol:camphor (7:3) are seen to be potential effective solvents for asphaltene dissolution.

4.3 Asphaltene Solubility in DESs

The best solvents from the computational screen were selected for experimental study, as depicted in Table S2. Figure S2 displays the chemical structures of HBA (thymol) and HBD's (camphor, decanoic acid, biphenyl, and diphenyl ether). The experimental solubility of asphaltene in four selected DESs was measured at room temperature and ambient pressure (Figure 5). DES1, composed of thymol-diphenyl ether, gives the highest asphaltene solubility, reaching a value of 43 ± 0.58 mg/mL at 298.15 K. This high solubility in DES1 is due to strong interactions between asphaltene and the DES1 components. The viscosities of the four solvents are given in Figure S3 DES1 possessing the lowest viscosity leads to a higher mass transfer rate for the solubility of asphaltene in the solvent. This leads to higher dispersion even at low temperatures. Intramolecular π−π interaction among asphaltene compounds within aromatic rings is known to lead to aggregation in crude oil [54, 55]. The aromatic ring compounds of HBA (*i.e.*, Thymol) and HBD initiate solvent interaction within the cyclo and phenyl rings of asphaltene. As a result, the intramolecular π−π interactions within the asphaltene compounds themselves are inhibited.

Further, the present study's asphaltene solubility results were compared with the literature. Asphaltene has been reported to be soluble in several solvents in a number of different research efforts [32, 55-59]. Asphaltene monomers, *i.e.*, without aggregation, have a solubility in toluene of 30 g/L[60]. 50 mg/L is the solubility at which asphaltene molecules start to form dimers[61], and asphaltene starts to aggregate at ~150 mg/L [62, 63]. The present study reveals

that DES show higher asphaltene solubilities than conventional organic solvents. According to the obtained results, the higher solubility capability order of DESs as follows: DES1 > DES2 > DES3 > DES4. However, the COSMO-RS predictions shows that DES2 have greater capability to dissolve asphaltene than DES1, this inconsistency between DES1 and DES2 is due to the higher viscosity of DES2.

4.4 Structural Characterisation through FTIR

The solubility and aggregation behaviour of asphaltene in the various solvents can be further understood by performing FTIR and NMR characterization techniques. Here, FTIR analysis was performed at different concentrations of asphaltene in DESs, to determine the change in functional group peak intensities of DES and asphaltene upon dissolution. The spectra were categorized into polar, diagnostic, and fingerprint regions, and are depicted in Figure 6. In the polar region the hydroxyl and amine groups are typically observed in the range of 3000 cm^{-1}-3600 cm^{-1}, corresponding to free or bonded pyrrolic N-H or bonded hydroxyl O-H stretching[59]. The free O-H/N-H groups available in solvents determine the hydrogen bonding with asphaltene and intensity decreases of these signals occur upon formation of hydrogen bonds between DESs and asphaltene. A detailed explanation of the free and bonded OH band IR stretching can be found elsewhere [56].

Figure 8 shows the spectra of different DESs with 20 mg asphaltene/mL DES. The likely location of the hydrogen-bonding band *i.e.*, 3200-3400 cm^{-1} was not investigated in this study, because of the difficulty in differentiating the corresponding contribution of the asphaltene-DES interactions from that from those arising from DES-DES or asphaltene-asphaltene interactions. Figure 9 shows the FTIR spectra of the DES free OH stretching band (~3520 cm^{-1}) peak at different concentrations of stabilized asphaltene. In order to use this 3520 cm^{-1} peak to study the DES-asphaltene interactions, the hydrogen bonding behaviour of asphaltene molecules themselves was investigated first. It has been reported that stronger intermolecular interaction between the asphaltene and DESs results in lower absorption intensity of free OH bonded stretching of DESs[56]. The absorbance intensity of 3520 cm^{-1} peak decreases with increasing concentration of asphaltene from 5 to 40 wt. %. This shows that the free OH stretching peak of DES decreases significantly with asphaltene concentration. It also indicates that the free OH in DES (with respect to the thymol moiety) forms hydrogen bonds with asphaltene.

In Figure 9 the lower peak intensity at 3100 cm^{-1}-3580 cm^{-1} is due to the interaction between the hydroxyl group of DES and the pyrrolic N-H group of asphaltene. DES1 and DES2 show lower absorption peak intensities of free OH of DESs and larger broadening of OH peaks than DES3 and DES4, indicating that DES1 and DES2 have stronger interactions with asphaltene than DES3 and DES4. This is in line with the experimental and COSMO-RS solubilities of these DES in asphaltene (Figure 4 and 6). FTIR spectra of asphaltene at three different concentrations in the presence of an amphiphile were reported by Chang *et al*. [56, 64] and a similar pattern was observed in that the addition of asphaltene causes a decrease in the peak intensity of free OH band stretch available at 3610 cm^{-1} due to the strong intermolecular interactions [56, 59].

4.5 Structural Characterisation of Asphaltene by NMR

The complex structure of asphaltene is a mixture of aliphatic, polycyclic aromatics, paraffinic, and olefinic compounds. Isotropic chemical shifts of ^{1}H NMR are shown in Figure 7. Table 2 reports the distribution of chemical shifts of the proton classifications (Table 2, H_A, H_α, H_β, H_γ, and H_N). These are classified based on the aliphatic and aromatic ring compounds in their immediate vicinity. The distribution of aromatic protons [H_{aro} (δ: 6.0-9.0)] and aliphatic protons H_{ali} (δ: 0-4.0) is depicted in The aliphatic region, in accordance with the previously published reports, has been further divided into three parts (a) H_α (δ:2.0-4.0) : protons attached to the saturated carbon in the α-position with respect to an aromatic ring,(b) H_β (δ : l.0-2.0): protons attached to paraffinic methylenes, naphthenes, methylene protons (β) ,and (c) H_γ (δ :0.5-1.0) : protons of paraffinic methyls (γ).

Peak areas of each specific type of proton in the ^{1}H NMR spectra were used to calculate the relative abundance of each species, as illustrated in table 2. The distributions were used to compute the ratio of hydrogen to carbon with the help of equation 5. The obtained H/C ratio for the particular compound was then compared to the theoretically calculated H/C ratio of the proposed model structures.

$$\frac{H}{C} = 3 \times CH_3 + 3 \times CH_2 + CH \quad (5)$$

Here CH_3, CH_2, and CH are the percentages of methyl, methylene, and methyne (including aromatic =C−H)) carbons present, respectively. The calculated H/C ratio (1.33) for model structure 2 was compared to the H/C ratio obtained from elemental analysis of ^{1}H NMR (1.30) to validate the asphaltene composition obtained using the integration of ^{1}H NMR (Table

3). A 97.7% agreement was obtained between the H/C values calculated from experimental analysis and quantum chemistry [65].

4.6 Asphaltene–DES Interactions using 2D-NOESY NMR

We also investigated the interactions between thymol-based DES and asphaltene at the molecular level using advanced 2D NMR techniques. Specifically, we used the {^{1}H–^{1}H} nuclear Overhauser effect (NOE) spectra to study short- and long-range spatial interactions between solvents and asphaltene, respectively. This involves assigning the specific chemical shifts for the hydrogen and carbon resonances detected in the ^{1}H and ^{13}C NMR spectra within a 2D representation to specific regions of the potential asphaltene structures (table 2, H_A, H_α, H_β, H_γ, and H_N). Figure 10 shows the interaction sites available between the components of DES1 (Thymol: Diphenyl Ether) and asphaltene with proton notation. Figure 11 shows the NMR analysis, which reveals ^{1}H–^{1}H interactions between DESs and asphaltene indicated by the contours above and below the diagonal, which are cross peaks (Figures 11a-11d). The peaks on the diagonal represent the interactions between the same molecules.

In Figure 11a, we observe a correlation between aromatic protons at 7.14 and 1.31 ppm. Also, a correlation between 1.29 and 0.92 ppm is assigned to aliphatic chain CH_2 and terminal CH_3. The signal at 3.22 ppm is assigned to the OH group bonded to the thymol of DES, and has two major correlations, one with 1.31 ppm (alicyclic CH_2) and the other with 1.40 ppm (aliphatic CH). The signal at 4.79 ppm is assigned to the H_N(NH) group bonded to the aromatic ring of the asphaltene, and has two correlations, with 1.71 ppm (alicyclic CH_2 group attached to thymol) and 1.40 ppm (aliphatic CH of HBD). The signal at 1.28 ppm is assigned to the CH_3 group attached to aromatic groups of DESs, and has two correlations, with 4.92 ppm (alicyclic CH_2) and 3.23 ppm (aliphatic CH). The correlation between 3.22 and 1.31 ppm proves the existence of the methyl proton CH_3–OH bonded to a hydroxyl group of thymol. We also observe correlations between protons of cyclohexanes with the proton attached to aromatic ring are of less intensity compared to aromatic carbon and proton of DESs signifying weaker interaction with asphaltene. The correlation between 4.92 and 1.71 ppm indicates the existence of H_N bonded with the alicyclic CH_2 group attached to thymol. This confirms hydrogen bonding between asphaltene and the DES. The resonance at 2.89 ppm, assigned to CH_2 of cyclohexane (α) to aromatic ring proton has two correlations, with 1.73 ppm (CH_2 at β) 1.40 ppm (aliphatic CH of a cyclic ring).

Hydrogen bonded interactions are also shown by FTIR analysis through figure 8-9 as discussed in the previous section. The on-diagonal peaks of the $^{1}H–^{1}H$ NOESY NMR at 6.5 and 8.03 ppm are assigned to aromatic hydrogen bonded to diphenyl ether, thymol and asphaltene. However, it is difficult to assign specific protons from asphaltene and DESs in aromatic regions due to overlapping of the peaks. The interaction of DES2 and DES3 also follows the same trend with decreases in cross peaks as HBD changes (see figure 11b). Here the aromatic region protons do not show any significant interaction or OH/NH peaks. The DES4 shows the fewest cross peaks which also confirms lowest solubility thereby indicating repulsive nature interaction by (i.e., long aliphatic chain present in decanoic acid) (figure 11d).

5. Conclusion

The present study aims to understand the complex molecular level structure and solubility mechanism of asphaltene in deep eutectic solvents. Theoretical DFT calculations were employed to obtain the structure of a model asphaltene compound based on the experimental FT-IR spectra of the asphaltene compound extracted from crude oil. Structure-2, based on the archipelago model, was found to be the closest to experiment, as the IR spectra highly resemble the FT-IR spectra of extracted asphaltene. Thereafter, the excess enthalpy and activity coefficient values for thymol-based solvents were predicted using the COSMO-RS model.

The FTIR and NMR spectra indicate that the solvation capacity of the DESs for the asphaltene is based on both hydrogen bonding and van der Waals dispersion energies. The solubility of asphaltene is primarily due to the van der Waals dispersion energies of the solvents and the donor-acceptor energies of the hydrogen bonds between the asphaltene molecule and the green solvents. The lower solubility of thymol: decanoic acid (3:2) is due to weaker van der Waals energies and reduced hydrogen-bond forming capacity. The asphaltene solubility was found to be lowest in DES4 (thymol: decanoic acid) because of the additional length of the alkyl chain in decanoic acid, which reduces its ability to prevent π–π interactions in asphaltene molecules, in contrast to other HBD which consist of polar aromatic rings. Overall, the outcome of the current approach helps us to understand the mechanism of asphaltene solubility and hence should aid in the development of targeted DESs for asphaltene dispersion in crude oil.

Acknowledgments

This work was part of the DOE Joint BioEnergy Institute (http:// www.jbei.org) supported by the U. S. Department of Energy, Office of Science, Office of Biological and Environmental Research, through contract DE-AC02-05CH11231 between Lawrence Berkeley National Laboratory and the U. S. Department of Energy. Support was also provided by the US Department of Energy (DOE), Office of Science, through the Genomic Science Program, Office of Biological and Environmental Research (contract no. FWP ERKP752). The United States Government retains and the publisher, by accepting the article for publication, acknowledges that the United States Government retains a non-exclusive, paid-up, irrevocable, worldwide license to publish or reproduce the published form of this manuscript, or allow others to do so, for United States Government purposes. The authors N. K. and T. B. would like to acknowledge the support of PARAM-ISHAN supercomputer facility for quantum calculation of IIT Guwahati. The author further acknowledges the Central Instrument of Facility (CIF) at the Indian Institute of Technology Guwahati for providing the FTIR and 600 MHz NMR facility.

Supporting Information

The COSMO-RS calculated activity coefficient and excess enthalpy of asphaltene DESs, prepared DESs, and the possible interactions of DES-asphaltene using the NMR spectra are provided in the supporting information.

Data Availability

Data will be made available on request.

Declaration of competing interest

The authors declare that they have no known competing financial interests or personal relationships that could have appeared to influence the work reported in this paper.

CRediT authorship contribution statement

Nikhil Kumar: Conceptualization, Methodology, Visualization, Formal analysis, Data curation, and Writing – original draft. **Mood Mohan:** Methodology, Visualization, Validation, Software, Formal analysis, Data curation, and Writing – review & editing. **Jeremy C. Smith:**

Writing – review & editing, Supervision, Funding acquisition. **Blake A. Simmons:** Writing – review & editing, Supervision, Resources, Funding acquisition. **Seema Singh:** Writing – review & editing, Resources, Supervision, Funding acquisition. **Tamal Banerjee:** Conceptualization, Writing – review & editing, Resources, Project administration, Supervision, Funding acquisition.

References

[1] F. Silva, M. Guimarães, P. Seidl, M. Garcia, Brazilian Journal of Petroleum and Gas 7 (2013).
[2] L.M. da Costa, S.R. Stoyanov, S. Gusarov, X. Tan, M.R. Gray, J.M. Stryker, R. Tykwinski, J.W. de M. Carneiro, P.R. Seidl, A. Kovalenko, Energy Fuels 26 (2012) 2727.
[3] P. Painter, M. Sobkowiak, J. Youtcheff, Fuel 66 (1987) 973.
[4] R. Zhao, R.-Q. Zhang, Physical Chemistry Chemical Physics 18 (2016) 25452.
[5] M. Anisimov, I. Yudin, V. Nikitin, G. Nikolaenko, A. Chernoutsan, H. Toulhoat, D. Frot, Y. Briolant, J Phys Chem 99 (1995) 9576.
[6] B.K. Wilt, W.T. Welch, J.G. Rankin, Energy Fuels 12 (1998) 1008.
[7] H. Wang, H. Xu, W. Jia, J. Liu, S. Ren, Energy Fuels 31 (2017) 2488.
[8] D.E. Scott, M. Schulze, J.M. Stryker, R.R. Tykwinski, Chem Soc Rev (2021).
[9] A. Hirschberg, L.N. deJong, B. Schipper, J. Meijer, Society of Petroleum Engineers Journal 24 (1984) 283.
[10] M.d.C. García, Energy Fuels 14 (2000) 1043.
[11] F. Mutelet, G. Ekulu, R. Solimando, M. Rogalski, Energy Fuels 18 (2004) 667.
[12] E. Buenrostro-Gonzalez, C. Lira-Galeana, A. Gil-Villegas, J. Wu, AIChE J 50 (2004) 2552.
[13] I. Moncayo-Riascos, F.A. Rojas-Ruiz, J.A. Orrego-Ruiz, C. Cundar, R.G. Torres, W. Cañas-Marín, Energy & Fuels 36 (2022) 837.
[14] M.R. Gray, R.R. Tykwinski, J.M. Stryker, X. Tan, Energy & Fuels 25 (2011) 3125.
[15] A.P. Abbott, G. Capper, D.L. Davies, R.K. Rasheed, V. Tambyrajah, ChemComm (2003) 70.
[16] M.A. Martins, S.P. Pinho, J.A. Coutinho, J Solut Chem 48 (2019) 962.
[17] N. Kumar, T. Banerjee, Industrial & Engineering Chemistry Research 61 (2022) 1464.
[18] P.K. Naik, N. Kumar, N. Paul, T. Banerjee, Deep Eutectic Solvents in Liquid-liquid Extraction: Correlation and Molecular Dynamics Simulation. CRC Press, 2022.
[19] N. Kumar, T. Banerjee, Journal of Chemical & Engineering Data 66 (2021) 3432.
[20] N. Kumar, P.K. Naik, T. Banerjee, The Journal of Physical Chemistry B 126 (2022) 4925.
[21] N. Kumar, P.K. Naik, T. Banerjee, Journal of Molecular Liquids 317 (2020) 113909.
[22] E.L. Smith, A.P. Abbott, K.S. Ryder, Chem. Rev. 114 (2014) 11060.
[23] B.B. Hansen, S. Spittle, B. Chen, D. Poe, Y. Zhang, J.M. Klein, A. Horton, L. Adhikari, T. Zelovich, B.W. Doherty, Chem. Rev. 121 (2021) 1232.
[24] A. Mohsenzadeh, Y. Al-Wahaibi, A. Jibril, R. Al-Hajri, S. Shuwa, Journal of Petroleum Science and Engineering 130 (2015) 6.

[25] F. Abu Hatab, O.A. Ibrahim, S.E. Warrag, A.S. Darwish, T. Lemaoui, M.M. Alam, T. Alsufyani, V. Jevtovic, B.-H. Jeon, F. Banat, ACS omega 8 (2022) 626.
[26] R. Timung, M. Mohan, B. Chilukoti, S. Sasmal, T. Banerjee, V.V. Goud, Biomass and Bioenergy 81 (2015) 9.
[27] Y. Chen, T. Mu, Green Chemical Engineering 2 (2021) 174.
[28] D. Yu, Z. Xue, T. Mu, Chemical Society Reviews 50 (2021) 8596.
[29] S. Kashefi, A. Shahrabadi, S. Jahangiri, M.N. Lotfollahi, H. Bagherzadeh, Energy Sources, Part A: Recovery, Utilization, and Environmental Effects 38 (2016) 3647.
[30] S. Jahangiri, A. Shahrabadi, A. Heydari, S. Javadian, A.H. Nazemi, S.M. Jahangiri, Petroleum Science and Technology 35 (2017) 1896.
[31] Z. Rashid, C.D. Wilfred, N. Gnanasundaram, A. Arunagiri, T. Murugesan, Journal of Molecular Liquids 255 (2018) 492.
[32] A. Sanati, M. Malayeri, O. Busse, J. Weigand, Journal of Molecular Liquids 334 (2021) 116100.
[33] R. Dennington, T. Keith, J. Millam, (2009).
[34] K. Huang, M. Mohan, A. George, B.A. Simmons, Y. Xu, J.M. Gladden, Green Chemistry 23 (2021) 6036.
[35] F. Eckert, A. Klamt, AIChE J 48 (2002) 369.
[36] M. Mohan, J.D. Keasling, B.A. Simmons, S. Singh, Green Chemistry (2022).
[37] E.C. Achinivu, M. Mohan, H. Choudhary, L. Das, K. Huang, H.D. Magurudeniya, V.R. Pidatala, A. George, B.A. Simmons, J.M. Gladden, Green Chemistry 23 (2021) 7269.
[38] M. Mohan, K. L. Sale, R.S. Kalb, B.A. Simmons, J.M. Gladden, S. Singh, ACS Sustainable Chemistry & Engineering 10 (2022) 11016.
[39] A.P. Abbott, D. Boothby, G. Capper, D.L. Davies, R.K. Rasheed, Journal of the American Chemical Society 126 (2004) 9142.
[40] J. Wang, J. Buckley, N.M.T. PRRC, Petroleum Recovery Research Center (2002).
[41] O.C. Mullins, Energy Fuels 24 (2010) 2179.
[42] I.A. Solov'yov, P.-Y. Chang, K. Schulten, Physical Chemistry Chemical Physics 14 (2012) 13861.
[43] K. Tsuji, K. Shibuya, The Journal of Physical Chemistry A 113 (2009) 9945.
[44] S. Badu, I.S. Pimienta, A.M. Orendt, R.J. Pugmire, J.C. Facelli, Energy & fuels 26 (2012) 2161.
[45] P. Larkin, Infrared and Raman spectroscopy: principles and spectral interpretation. Elsevier, 2017.
[46] N.V. Chukanov, A.D. Chervonnyi, Infrared spectroscopy of minerals and related compounds. Springer, 2016.
[47] C. Baldrich, B. Murcia, A. Bueno, CT&F-Ciencia, Tecnología y Futuro 3 (2006) 149.
[48] M. Mohan, V.V. Goud, T. Banerjee, Fluid Phase Equilib. 395 (2015) 33.
[49] J.M. Prausnitz, R.N. Lichtenthaler, E.G. De Azevedo, Molecular thermodynamics of fluid-phase equilibria. Pearson Education, 1998.
[50] M. Mohan, C. Balaji, V.V. Goud, T. Banerjee, J. Solution Chem. 44 (2015) 538.
[51] M. Mohan, P. Viswanath, T. Banerjee, V.V. Goud, Mol. Phys. 116 (2018) 2108.
[52] M. Mohan, T. Banerjee, V.V. Goud, Journal of Chemical and Engineering Data 61 (2016) 2923.
[53] M. Mohan, J.D. Keasling, B.A. Simmons, S. Singh, Green Chem. (2022) 4140.
[54] Z. Rashid, C.D. Wilfred, N. Gnanasundaram, A. Arunagiri, T. Murugesan, Journal of Petroleum Science and Engineering 176 (2019) 249.
[55] Y. Zhang, M. Siskin, M.R. Gray, C.C. Walters, R.P. Rodgers, Energy & Fuels 34 (2020) 9094.

[56] C.-L. Chang, H.S. Fogler, Langmuir 10 (1994) 1758.
[57] N. Haji-Akbari, P. Teeraphapkul, H.S. Fogler, Energy & fuels 28 (2014) 909.
[58] O.P. Strausz, T.W. Mojelsky, E.M. Lown, Fuel 71 (1992) 1355.
[59] I. Zojaji, A. Esfandiarian, J. Taheri-Shakib, Advances in Colloid and Interface Science 289 (2021) 102314.
[60] A.B. Andrews, R.E. Guerra, O.C. Mullins, P.N. Sen, The Journal of Physical Chemistry A 110 (2006) 8093.
[61] S. Goncalves, J. Castillo, A. Fernandez, J. Hung, Fuel 83 (2004) 1823.
[62] G. Andreatta, N. Bostrom, O.C. Mullins, Langmuir 21 (2005) 2728.
[63] G. Andreatta, C.C. Goncalves, G. Buffin, N. Bostrom, C.M. Quintella, F. Arteaga-Larios, E. Pérez, O.C. Mullins, Energy Fuels 19 (2005) 1282.
[64] B. Athokpam, S.G. Ramesh, R.H. McKenzie, Chemical Physics 488 (2017) 43.
[65] M.U. Hasan, M.F. Ali, A. Bukhari, Fuel 62 (1983) 518.

Table 1. Elemental composition of the asphaltene model compounds and compares the results with literature reported chemical structures.

Asphaltene type	C	H	N	O	S	H/C atomic ratio	Reference
Model 1 (Asphaltene_island)	71.38	4.03	5.56	19.03		0.66	Present study
Model 2 (Campana)	87.16	8.61	1.29	2.94		1.18	Present study
Model 3 (Mid New)	85.50	9.30	1.16	1.34	2.70	1.23	Present study
	83.88	11.35	0.37	2.64	1.76	1.62	Salih et al. (2019 [68]
Liaohe	86.32	8.30	2.19	2.91	0.29	1.16	Zheng et al. (2017) [69]
Vene	82.85	7.93	1.82	2.35	5.06	1.15	Zheng et al. (2017) [69]
	83.3	7.8	1.2	7.7		1.12	Soleymani et al. (2008) [70]
	83.3	8.2	2.1	2.6	1.2	1.18	Marques et al. (2012) [71]

Table 2. Classification of ^{1}H NMR spectra based on the different types of significant proton types attached to the asphaltene compound [44, 65].

Chemical Shift Ranges (ppm)	**Symbol**	**Type of Hydrogen**
6.0-9.0	H_A	aromatic protons
6.0-4.0	H_N	naphthenic and porpyrinic CH/CH_2 groups
2.1-4.0	H_α	aliphatic hydrogen in α position to an aromatic ring
1.0-2.1	H_β	aliphatic hydrogen in β position or further from aromatic; methylene/methyne hydrogen in alkane
0.5-1.0	H_γ	methyl hydrogen in γ or further from the aromatic ring; methyl hydrogen in alkane

Table 3. ^{1}H NMR spectra analysis for the composition of pure asphaltene sample.

Sample Name	H_A	H_α	H_β	H_γ	H_N
Asphaltene	19.97	12.29	64.53	2.78	0.43

(a) Model structure 1

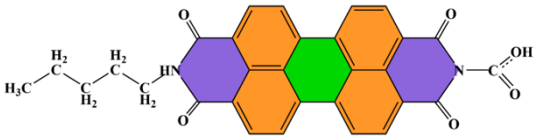

(b) Model structure 2

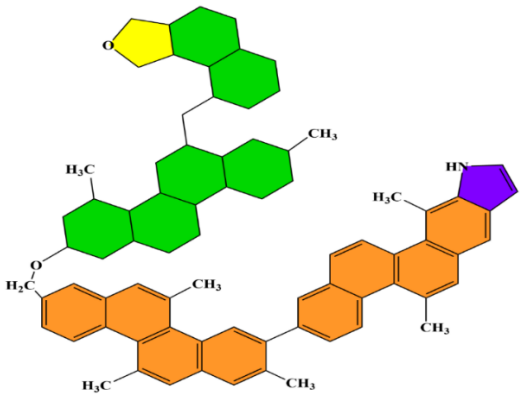

(c) Model structure 3

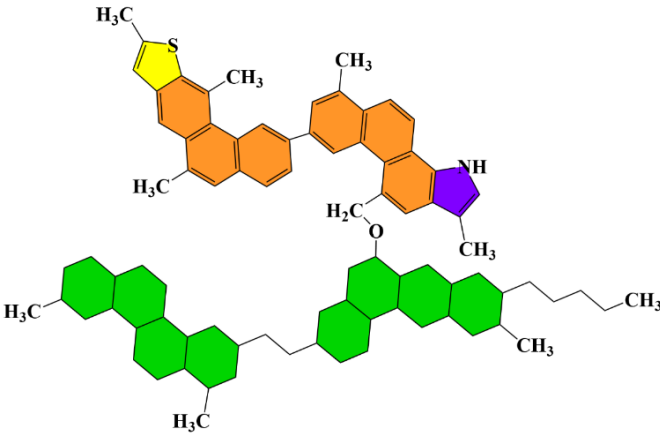

Figure 1. The different model structures of asphaltene used for screening of potential DESs. The COSMO cavities of these structures are provided in supporting information Figure S1. Here green color represents cyclic ring and orange color indicates aromatic rings, violet color represents the amine-based ring structure and yellow color represents the heteroatom cyclic ring.

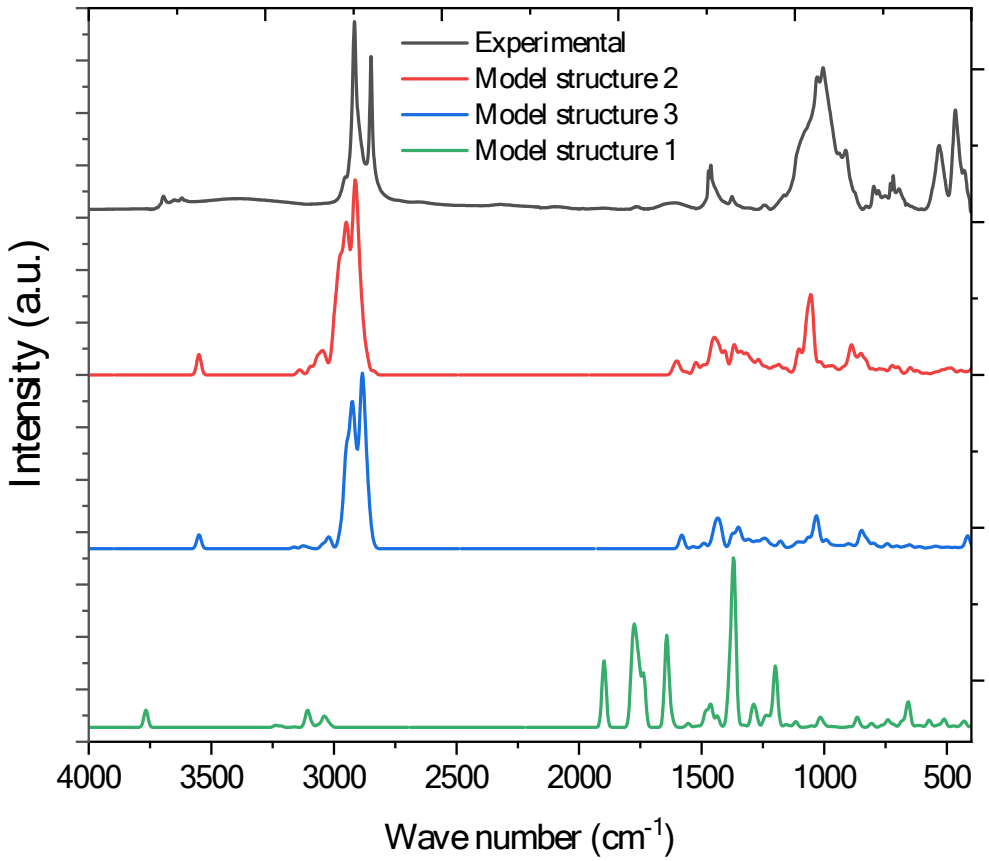

Figure 2. The correlation between quantum chemical calculated and experimental IR spectra of asphaltene with different starting model structures of asphaltene. DFT calculations were calculated at B3LYP theory and 6-311+G (d, p) basis set.

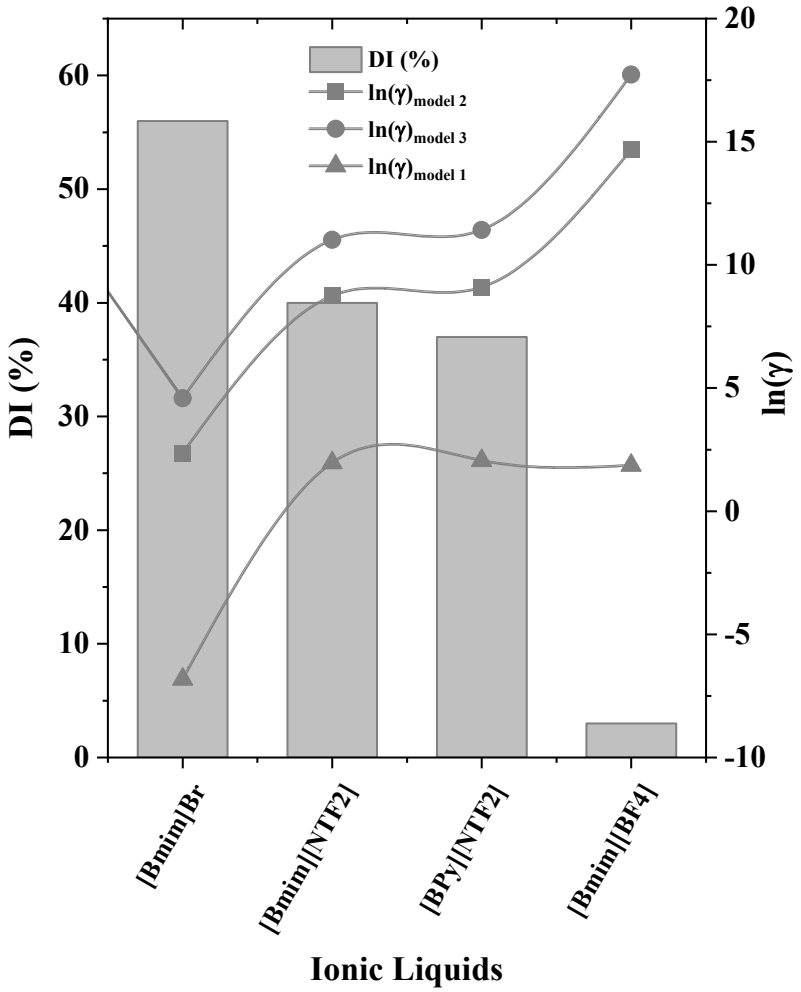

Figure 3. Experimental solubility of asphaltene *vs* COSMO-RS predicted logarithmic activity coefficient (*ln* (*γ*)) of different asphaltene model structures in ionic liquids.

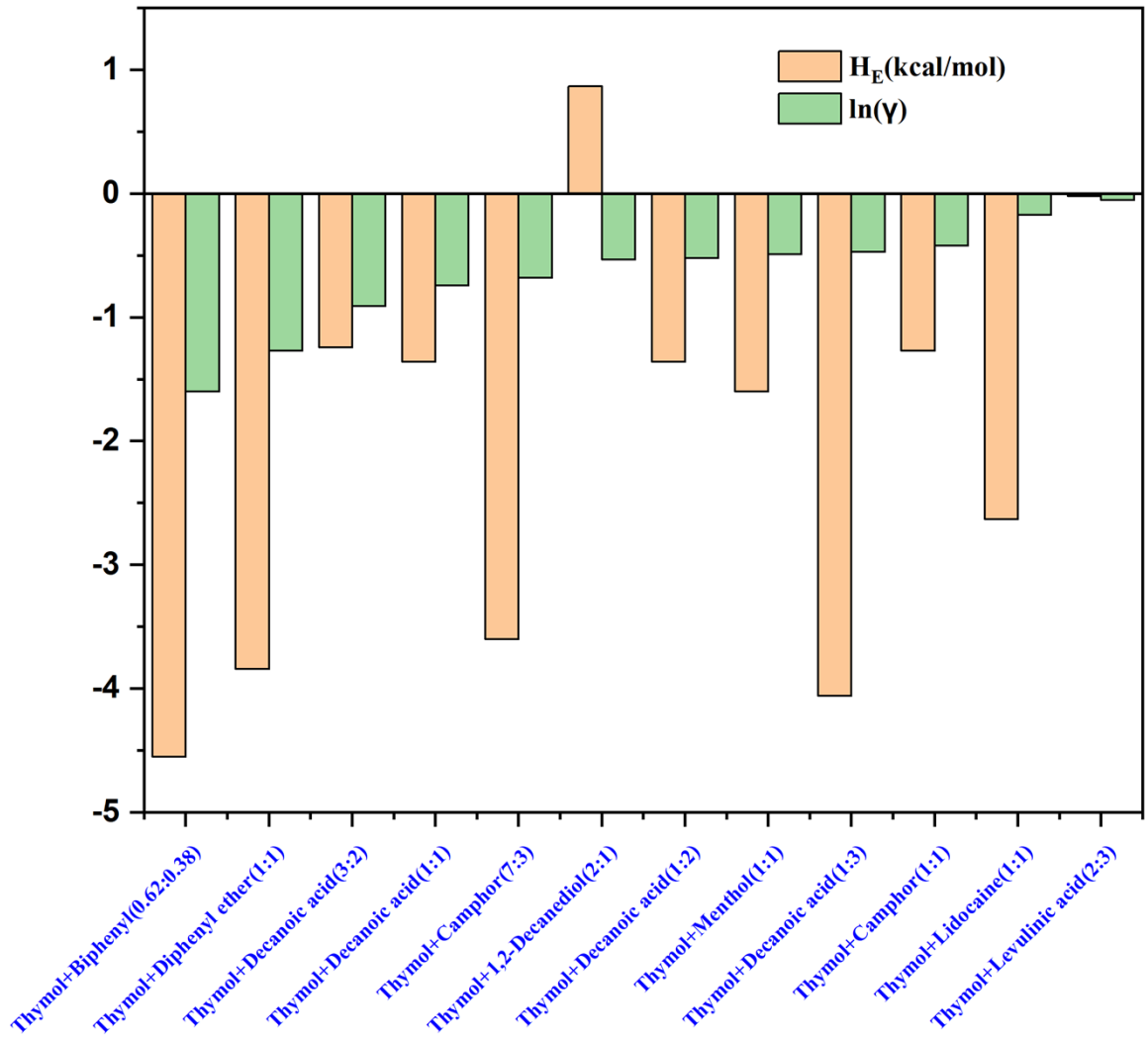

Figure 4. COSMO-RS predicted excess enthalpy and logarithmic activity coefficients of asphaltene for model 2 structure.

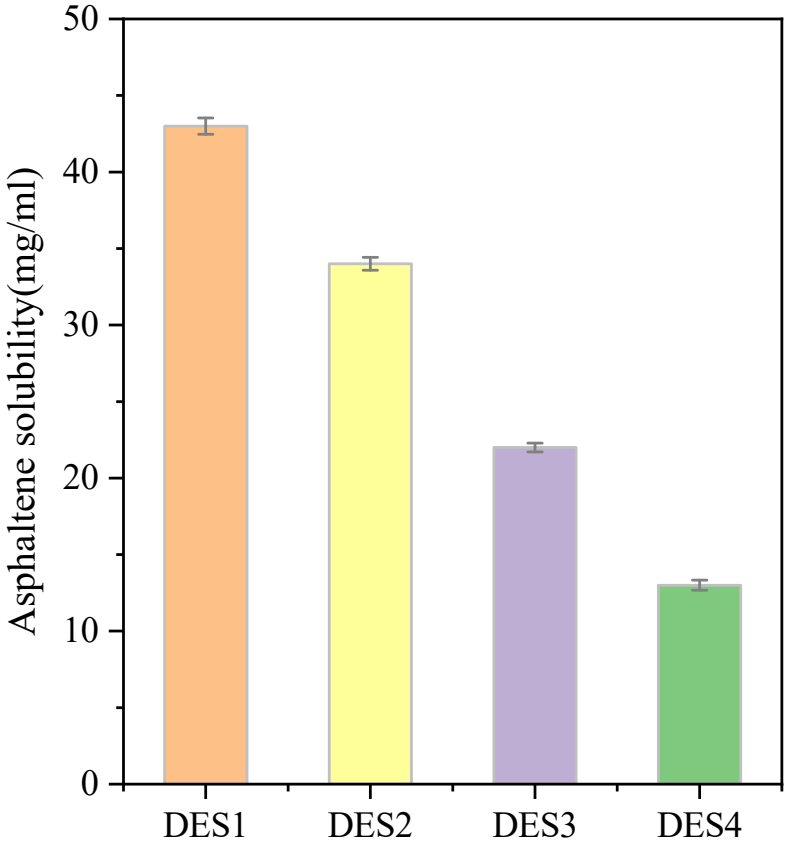

Figure 5. Solubility of asphaltene in different DESs at 298.15 K and ambient pressure. Error bars represent the standard deviation calculated from three independent experiments ($p = 0.05$). Significant differences between groups ($p < 0.05$) are indicated with lowercase letters.

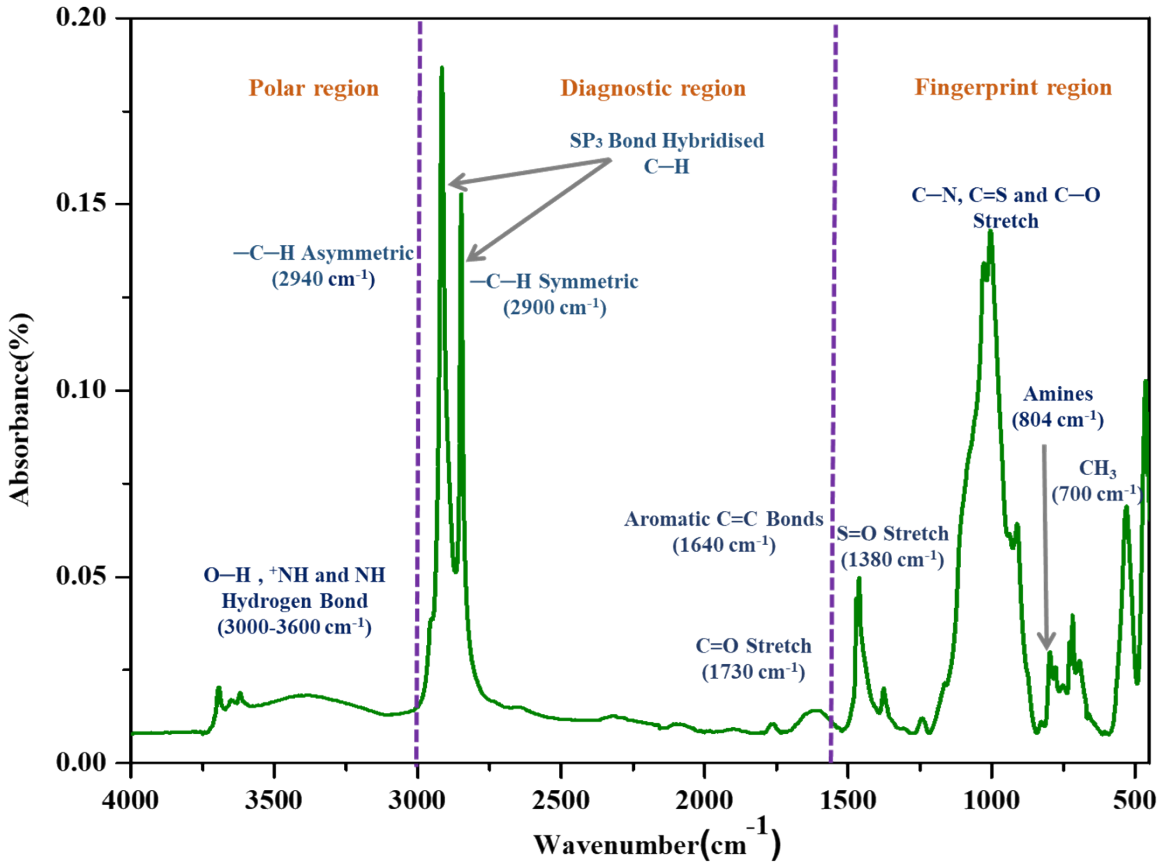

Figure 6. The FTIR characterization of asphaltene compound extracted from the crude oil.

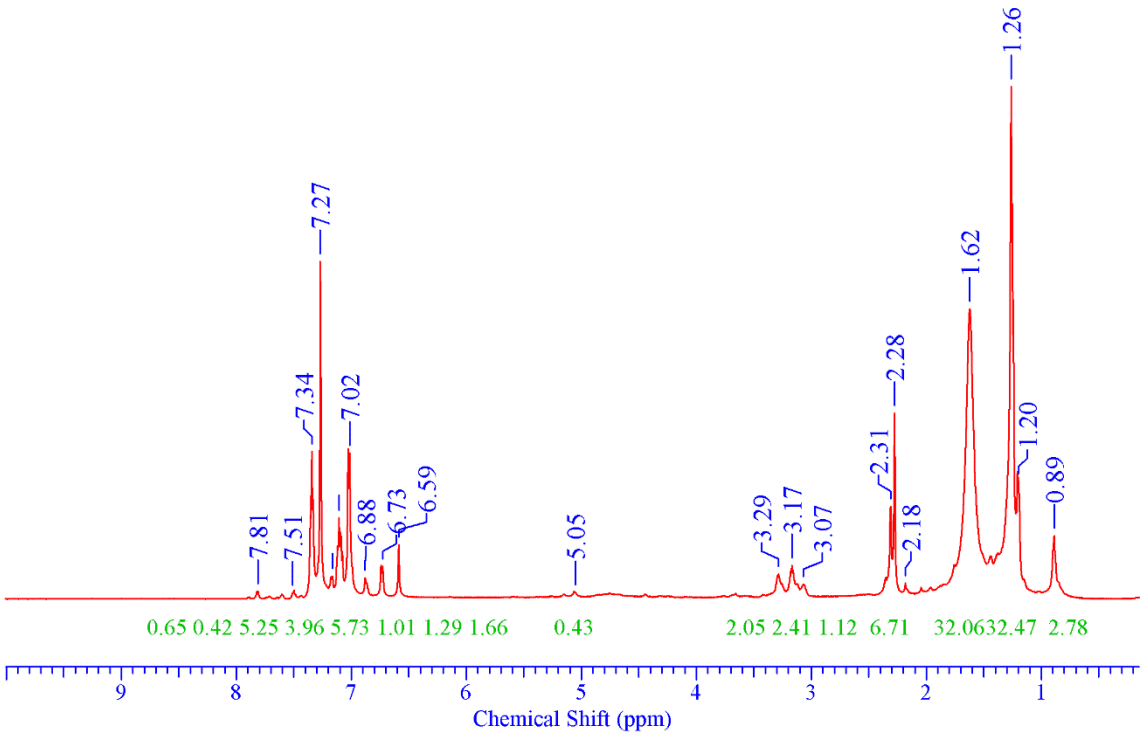

Figure 7. ^{1}H NMR of pure Asphaltene compound used in this study with integral values.

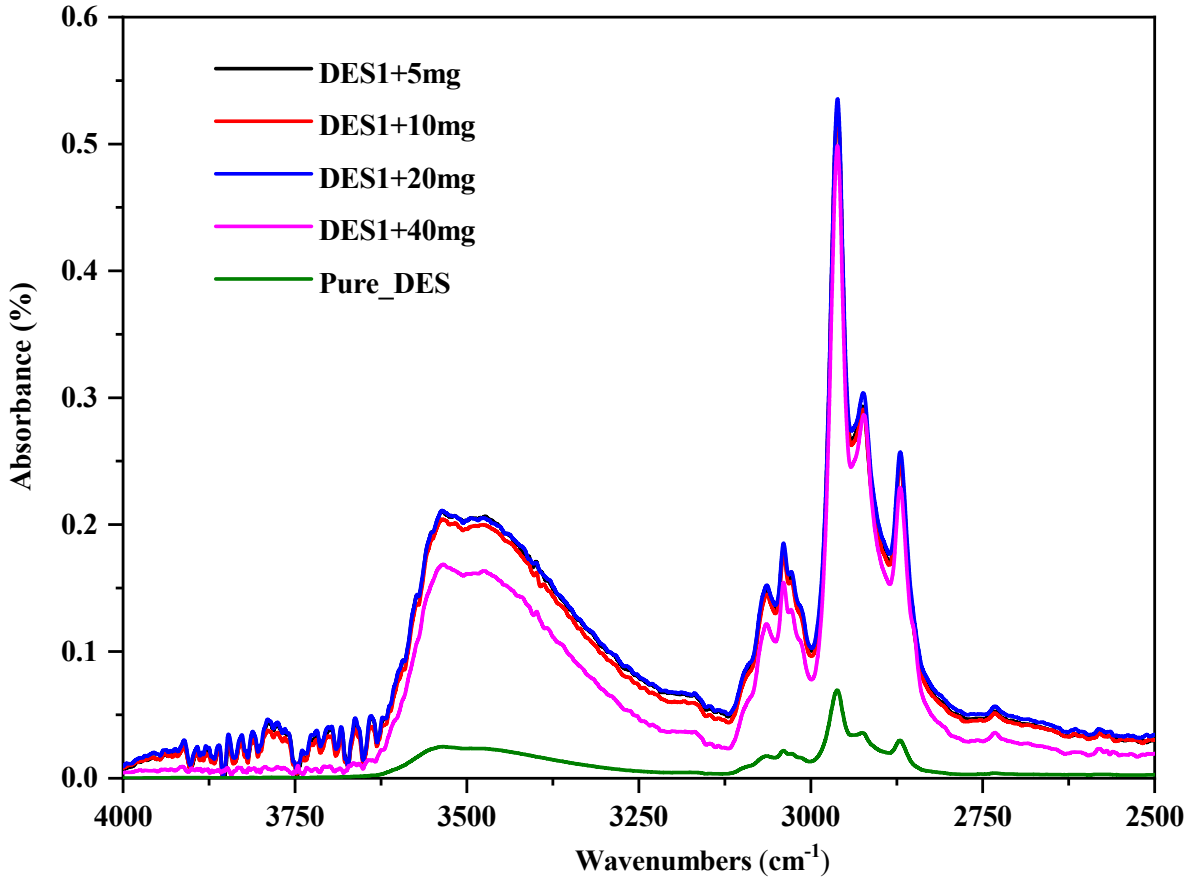

Figure 8. Comparison of the FTIR spectra of the asphaltene sample at four different mass fractions in DES1 with neat DES1.

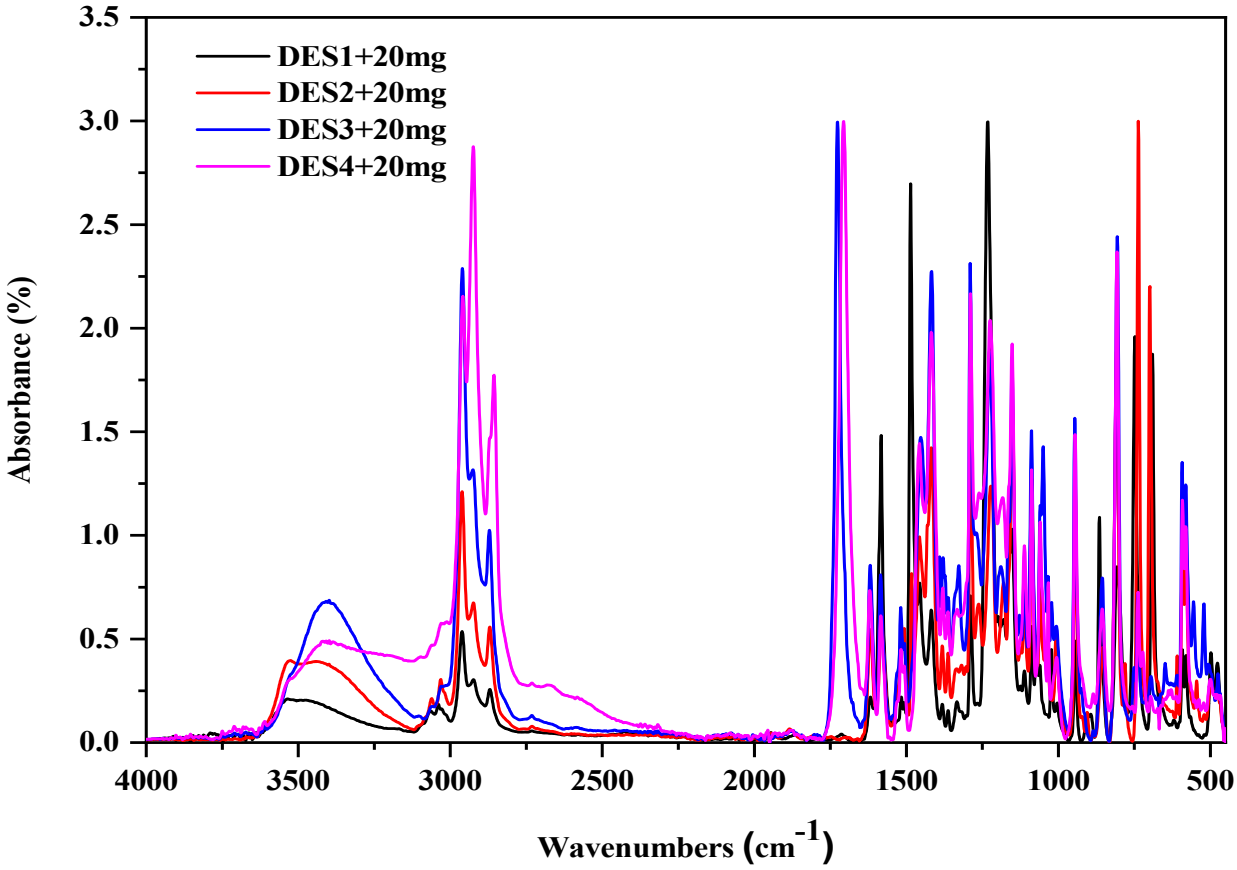

Figure 9. The FTIR spectra of asphaltene after solubilization in different DESs.

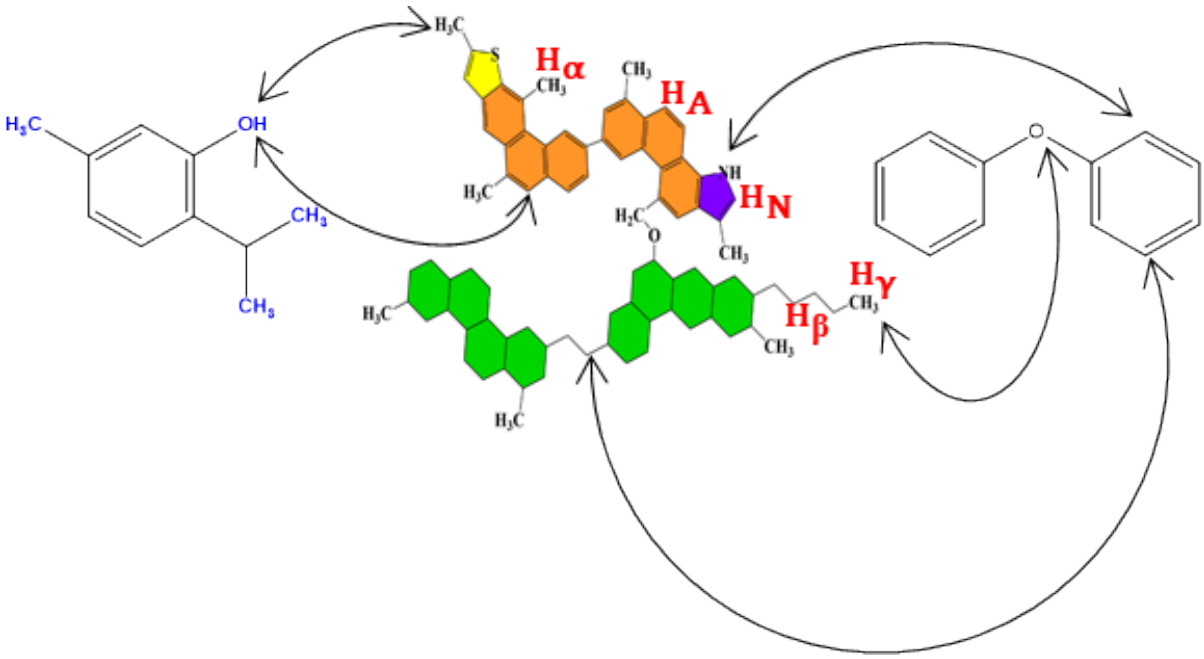

Figure 10. The schematic diagram representing the interaction sites for the 2D-NMR of asphaltene interaction with the DES1 (Thymol: Diphenyl Ether).

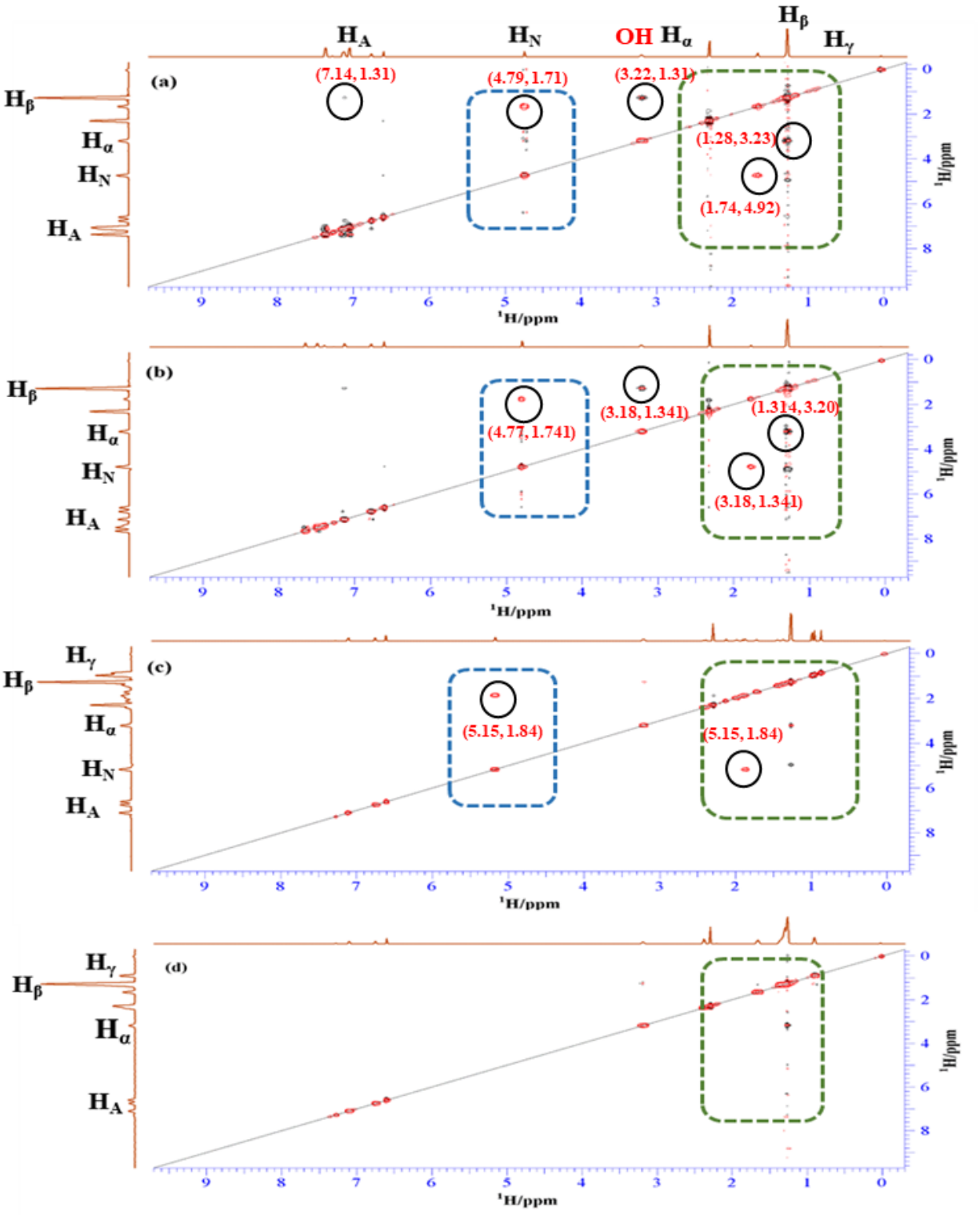

Figure 11. Representative NOESY (^{1}H-^{1}H) NMR spectra of asphaltene dissolved in DESs (a) DES1+ASP (b) DES2+ASP (c) DES3+ASP (d) DES4+ASP.